PNAS RESEARCH ARTICLE | NEUROSCIENCE OPEN ACCESS

$GABA_B$ receptors induce phasic release from medial habenula terminals through activity-dependent recruitment of release-ready vesicles

Peter Koppensteiner[a,1,2], Pradeep Bhandari[a,1], Cihan Önal[a,1], Carolina Borges-Merjane[a,3], Elodie Le Monnier[a], Utsa Roy[a], Yukihiro Nakamura[b], Tetsushi Sadakata[c], Makoto Sanbo[d], Masumi Hirabayashi[d], JeongSeop Rhee[e], Nils Brose[e], Peter Jonas[a], and Ryuichi Shigemoto[a,2]

Edited by Thomas Südhof, Stanford University, Stanford, CA; received January 26, 2023; accepted January 3, 2024

$GABA_B$ receptor (GBR) activation inhibits neurotransmitter release in axon terminals in the brain, except in medial habenula (MHb) terminals, which show robust potentiation. However, mechanisms underlying this enigmatic potentiation remain elusive. Here, we report that GBR activation on MHb terminals induces an activity-dependent transition from a facilitating, tonic to a depressing, phasic neurotransmitter release mode. This transition is accompanied by a 4.1-fold increase in readily releasable vesicle pool (RRP) size and a 3.5-fold increase of docked synaptic vesicles (SVs) at the presynaptic active zone (AZ). Strikingly, the depressing phasic release exhibits looser coupling distance than the tonic release. Furthermore, the tonic and phasic release are selectively affected by deletion of synaptoporin (SPO) and Ca^{2+}-dependent activator protein for secretion 2 (CAPS2), respectively. SPO modulates augmentation, the short-term plasticity associated with tonic release, and CAPS2 retains the increased RRP for initial responses in phasic response trains. The cytosolic protein CAPS2 showed a SV-associated distribution similar to the vesicular transmembrane protein SPO, and they were colocalized in the same terminals. We developed the "Flash and Freeze-fracture" method, and revealed the release of SPO-associated vesicles in both tonic and phasic modes and activity-dependent recruitment of CAPS2 to the AZ during phasic release, which lasted several minutes. Overall, these results indicate that GBR activation translocates CAPS2 to the AZ along with the fusion of CAPS2-associated SVs, contributing to persistency of the RRP increase. Thus, we identified structural and molecular mechanisms underlying tonic and phasic neurotransmitter release and their transition by GBR activation in MHb terminals.

medial habenula | $GABA_B$ receptor | vesicle release | Flash and Freeze | Flash and Freeze-fracture

Significance

The enhancement of neurotransmission from medial habenula terminals by γ-aminobutyric acid type B ($GABA_B$) receptor (GBR) activation is the strongest known potentiation of transmitter release in the central nervous system, but the underlying mechanisms remain enigmatic. We found that this potentiation is associated with a transition from facilitating tonic to depressing phasic mode of release caused by GBR- and activity-dependent recruitment of release-ready vesicles at a looser coupling distance than the tonic-release vesicles. CAPS2 (Ca^{2+}-dependent activator protein for secretion 2) retains these vesicles there for minutes contributing to a persistent potentiation. Thus, we provide insights into the mechanisms underlying a new form of presynaptic modulation at a central synapse.

The synaptic connection from the medial habenula (MHb) to the interpeduncular nucleus (IPN) is a phylogenetically conserved pathway involved in emotion- and addiction-related behaviors (1–3). The most striking peculiarity in this pathway is a massive enhancement of neurotransmitter release from terminals originating from cholinergic neurons in the ventral MHb by activation of presynaptic $GABA_B$ receptors (GBRs) (2), usually inhibitory G-protein-coupled receptors (4–7). It is currently unclear which mechanisms mediate this increase in release. Another unique feature of the MHb-IPN synapse is the exclusive use of Cav2.3 for release (8). However, Cav2.3-mediated release is not necessarily potentiated by GBR activation since it is inhibited in terminals originating in the dorsal MHb (8, 9).

The repeated excitation of synaptic terminals results in either facilitation or depression of neurotransmitter release, also called tonic and phasic release, respectively (10–12). While the depression of phasic release is most commonly mediated by the depletion of the readily releasable pool (RRP) of synaptic vesicles (SVs), the facilitation of tonic release is likely mediated by a progressive increase in release probability (P_r), for example by residual Ca^{2+} (10, 13). Although the molecular properties determining the release modes in each synapse type are incompletely understood, relevant factors include Ca^{2+} influx, stimulation frequency, and the priming/docking states of SVs (10–12, 14).

Here, we report that following GBR activation, MHb terminals transition from a facilitating, tonic to a depressing, phasic neurotransmitter release mode at a physiological stimulation frequency (15–17). This transition is induced by an increase in Ca^{2+} influx, which recruits additional SVs to the RRP. Using "Flash and Freeze" in acute IPN slices (18), we observed an activity-dependent increase in docked SVs following GBR activation to the same extent as the increase in RRP size. We found two proteins colocalized in MHb terminals, synaptoporin (SPO) and Ca^{2+}-dependent activator protein for secretion 2 (CAPS2), selectively involved in tonic and phasic release, respectively. We developed a

Author contributions: P.K. and R.S. designed research; P.K., P.B., C.Ö., E.L.M., and U.R. performed research; C.Ö., C.B.-M., T.S., M.S., M.H., J.R., N.B., and P.J. contributed new reagents/analytic tools; P.K., P.B., E.L.M., and Y.N. analyzed data; and P.K., P.J., and R.S. wrote the paper.

The authors declare no competing interest.

This article is a PNAS Direct Submission.

[1]P.K., P.B., and C.Ö. contributed equally to this work.

[2]To whom correspondence may be addressed. Email: peter.koppensteiner@ist.ac.at or ryuichi.shigemoto@ist.ac.at.

[3]Present address: Biozentrum of the University of Basel, 4056 Basel, Switzerland.

This article contains supporting information online at https://www.pnas.org/lookup/suppl/doi:10.1073/pnas.2301449121/-/DCSupplemental.

Published February 12, 2024.

method for nanoscale visualization of membrane-associated proteins within milliseconds after exocytosis, termed "Flash and Freeze-fracture," and found CAPS2 recruitment to the presynaptic active zone (AZ) during phasic release. In conclusion, we identified a transition from tonic to phasic release by GBR activation in MHb terminals as a new form of presynaptic modulation mediated via unique molecular and structural mechanisms.

Results

Transition from Tonic to Phasic Neurotransmitter Release by GBR Activation. Since rodent MHb neurons are active at ~10 Hz in vivo (15–17), we measured excitatory postsynaptic currents (EPSCs) in whole-cell configuration evoked by repetitive stimulation of MHb axons at this physiological frequency in rostral/central IPN neurons. In order to keep the MHb-IPN pathway through the fasciculus retroflexus (FR) intact, we prepared 1-mm-thick angled slices as described previously (8) (Fig. 1*A*). Under baseline conditions, at 2.5 mM external Ca^{2+} concentration, 10-Hz stimulation for 3 s produced EPSC responses that increased in amplitude with consecutive stimuli (Fig. 1*B*). Application of the GBR agonist R(+)-baclofen (1 μM) markedly potentiated initial EPSC amplitudes in the 10-Hz train but continued stimulation progressively reduced subsequent EPSC amplitudes (Fig. 1 *B*–*D*). Normalization of EPSC amplitudes to the corresponding first baseline EPSC at control conditions revealed that the enhanced EPSC amplitudes by baclofen decayed to the level of the facilitated baseline EPSC amplitudes (Fig. 1*D*). This implies that tonic and phasic release exhibit similar release rates during prolonged activity (19). Importantly, baclofen still potentiated release at 1 mM external Ca^{2+} concentration (*SI Appendix*, Fig. S1 *A* and *B*). Thus, MHb terminals exhibited a facilitating, tonic neurotransmitter release pattern under baseline conditions and transitioned to a depressing, phasic release pattern after GBR activation at a physiological Ca^{2+} concentration.

Ventral MHb terminals corelease glutamate and acetylcholine (20). Therefore, we tested whether tonic and phasic release were selectively mediated by one of the two transmitters. Cholinergic EPSC trains in the presence of the α-amino-3-hydroxy-5-methyl-4-isoxazolepropionic acid (AMPA) receptor blocker DNQX (10 μM) still transitioned to a phasic response pattern after GBR activation (*SI Appendix*, Fig. S1*C*) similar to that of glutamatergic EPSC trains in the presence of cholinergic receptor blockers (50 μM hexamethonium and 5 μM mecamylamine) (*SI Appendix*, Fig. S1*D*). Although the RRP determined by cumulative EPSC analysis in the presence of DNQX (0.72 ± 0.18 nA, n = 8 cells) was much smaller than that in the presence of cholinergic blockers (3.57 ± 0.47 nA, n = 8 cells; *SI Appendix*, Fig. S1*E*), P_r values were not significantly different (*SI Appendix*, Fig. S1*E*). Thus, the GBR-mediated phasic release induction equally affects cholinergic and glutamatergic release, though glutamate mainly contributes to the EPSCs.

We then quantified the recovery from activity-dependent modulations of tonic and phasic release (Fig. 1 *E* and *F*). Measuring from peak increase at 1.3 s after 10 Hz, the facilitated baseline responses decayed exponentially with a time constant (τ) of 6.9 s (Fig. 1*G*), suggesting that this increase is kinetically similar to augmentation (21–23). Similarly, depression of phasic release recovered with a τ

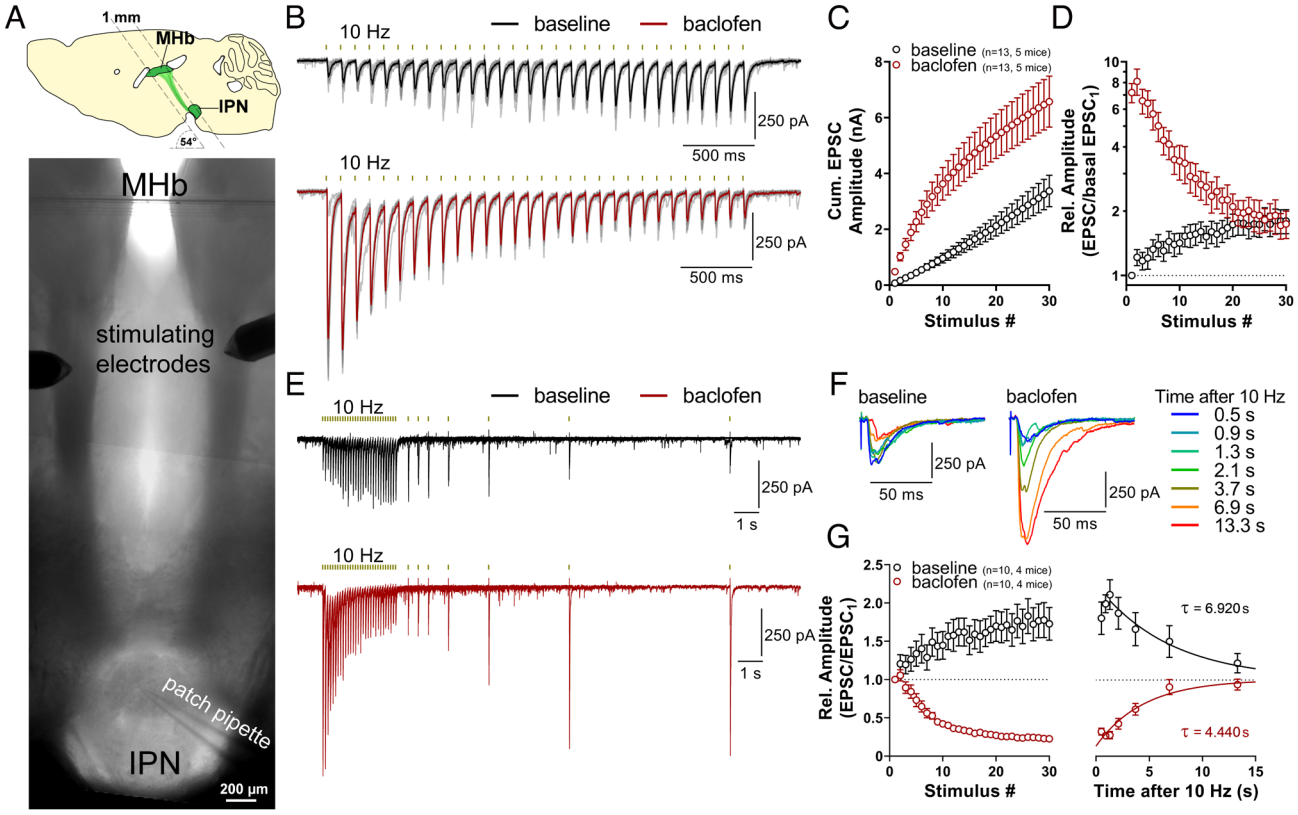

Fig. 1. Stimulation of MHb axons at a physiological frequency reveals transition from tonic to phasic neurotransmitter release by baclofen. (*A*) Scheme of the 1-mm-thick angled slice preparation (*Top*) and an example of the recording configuration in the resulting slice (*Bottom*). (*B*) Example traces of EPSCs evoked by 10-Hz stimulation in one cell before and after the application of baclofen (1 μM). Grayed responses represent individual sweeps (including the very first stimulation under each condition), and bold responses represent the average of the individual traces. (*C*) Quantification of baseline and baclofen responses using cumulative EPSC amplitudes. (*D*) Plot of EPSC responses after normalization to the amplitude of the corresponding first baseline EPSC. (*E*) Overlay of 7 traces of 10-Hz responses at baseline and during baclofen in one cell with single stimulations at varying intervals following the 10-Hz stimulus. (*F*) Overlay of single stimuli color-coded with stimulation time. (*G*) Quantification of recovery from tonic and phasic activity-dependent modulations. Using exponential fit, both short-term plasticity exhibited recovery times in the order of seconds. See also *SI Appendix*, Figs. S1 and S2.

of 4.4 s, suggesting that the EPSC decrease results from RRP depletion and not from Cav2.3 channel inactivation (24).

Molecular Signaling Mechanisms Underlying GBR-Mediated Potentiation. We next investigated the GBR-mediated signaling mechanisms underlying the induction of phasic release. Since GBRs are coupled to inhibitory G-proteins, we tested noncanonical signaling involving cyclic adenosine monophosphate/protein kinase A (cAMP/PKA) or phospholipase C/protein kinase C (PLC/PKC) signaling pathways (*SI Appendix*, Fig. S2). The application of the adenylyl cyclase activator forskolin (20 μM) did not significantly affect tonic release and the transition to phasic release by baclofen (*SI Appendix*, Fig. S2*A*). Similarly, PKA inhibitor KT5720 (1 μM) did not affect the potentiation of release by baclofen (*SI Appendix*, Fig. S2*B*).

Ventral MHb neurons express a rare PLC subunit, PLCη2 (25), which has the highest Ca^{2+} sensitivity among all known PLC subunits (26). Presynaptic PLCη2 may be constitutively active, and its GBR-mediated inhibition could cause a rapid accumulation of phosphatidylinositol 4,5-bisphosphate (PIP_2) in the presynaptic membrane, thereby increasing exocytosis via PIP_2-dependent effectors (27). However, we found no changes in the baclofen effect in PLCη2 knockout mice (*SI Appendix*, Fig. S2*C*) or in the presence of the PLC inhibitor U73122 (10 μM; *SI Appendix*, Fig. S2*E*). Alternatively, PKC phosphorylation could enhance the Cav2.3 conductance as previously reported (28). However, neither the PKC activator phorbol 12-myristate 13-acetate (1 μM; *SI Appendix*, Fig. S2*D*) nor the diacylglycerol analogue 1,2-Dioctanoyl-sn-glycerol (20 μM; *SI Appendix*, Fig. S2*F*) affected the induction of phasic release by baclofen. Thus, it is unlikely that cAMP/PKA and PLC/PKC pathways are involved in the GBR-mediated potentiation.

Role of Presynaptic Ca^{2+} in the GBR-Mediated Enhancement of Neurotransmitter Release. We next explored the role of presynaptic Ca^{2+} in the GBR-mediated induction of phasic release. Using AAV injections into the MHb of ChAT-IRES-Cre mice, we expressed axon-GCaMP6s in cholinergic neurons. FR stimulation at 10 Hz for 3 s increased presynaptic GCaMP6s fluorescence in the IPN 4.0 ± 0.6-fold in control vs. 6.5 ± 0.9-fold in baclofen (n = 5 slices, 5 mice; Fig. 2 *A* and *B*). However, presynaptic GBRs are known to inhibit Ca^{2+} influx through voltage-gated Ca^{2+} channels (VGCCs) and no report shows GBR-mediated increases in Ca^{2+} influx for any VGCCs in reconstituted systems (5, 29–31). Using simulations based on our Ca^{2+} imaging data, we asked whether the increase in presynaptic Ca^{2+} could arise from the inhibition of the Ca^{2+}-binding ability of a buffer rather than enhanced Ca^{2+} influx (*SI Appendix*, Fig. S3 and Table S1). Response kinetics of our experimental GCaMP6s data showed significantly faster rise times after baclofen application with no change in decay times (*SI Appendix*, Fig. S3 *A–D*). Using GCaMP6s as a model buffer, we simulated Ca^{2+} response kinetics at distinct buffer concentrations. We found that high concentrations of a high-affinity Ca^{2+} buffer resulted in significantly prolonged decay times and lower peak fluorescence (*SI Appendix*, Fig. S3 *E–H*), ruling out Ca^{2+} unbuffering as the GBR-mediated mechanism. Furthermore, alterations in Ca^{2+} extrusion also failed to reproduce the observed changes in GCaMP6s fluorescence after baclofen (*SI Appendix*, Fig. S3 *I* and *J*). Finally, we found that a 2.3-fold increase in Ca^{2+} influx most closely reproduced our observed increase in GCaMP6s peak fluorescence after baclofen (*SI Appendix*, Fig. S3 *K–M*).

Since our simulation was consistent with increased Ca^{2+} influx as the cause of the GBR-mediated increase in presynaptic GCaMP6s fluorescence, we next tested whether increasing Ca^{2+} influx by other means was sufficient to induce phasic release. Surprisingly, bath application of the voltage-gated K^+ channel blockers tetraethylammonium chloride (TEA-Cl, 1 mM) and 4-aminopyridine (4-AP, 100 μM) neither induced phasic release nor occluded its induction by baclofen (Fig. 2 *C–E*). Although TEA/4-AP application enhanced spontaneous neurotransmitter release, evoked EPSC responses remained tonic. We then performed Ca^{2+} imaging and confirmed that applying TEA/4-AP strongly enhanced presynaptic Ca^{2+} influx and the spontaneous activity of MHb axons (Fig. 2 *F* and *G*). However, adding baclofen did not further enhance the peak GCaMP6s fluorescence, suggesting that TEA/4-AP increased presynaptic Ca^{2+} influx similarly to baclofen. Therefore, we conclude that increasing Ca^{2+} influx alone is insufficient to induce phasic release. An important consideration of our Ca^{2+} imaging experiments is the nonlinearity and potential saturation of GCaMP6s fluorescence (32) by excessive Ca^{2+} influx, particularly in the TEA/4-AP experiment (Fig. 2*F*).

Based on the above result, we hypothesized that increased Ca^{2+} influx during phasic release might result in the diffusion of Ca^{2+} to recruit additional SVs more distant from the Ca^{2+} channel. Therefore, we tested the effect of a slow membrane-permeable Ca^{2+} chelator, ethyleneglycol- bis(β-aminoethyl)-N,N,N′,N′-tetraacetoxymethyl ester (EGTA-AM, 100 μM), on phasic release, applied after baclofen (Fig. 2 *H–J*). EGTA-AM reduced the first EPSC ($EPSC_1$) amplitude on average by 51.8 ± 2.1% (Fig. 2*J*; n = 8 cells, 4 mice), suggesting that the phasic release is loosely coupled to Cav2.3 (33). In contrast, EGTA-AM had no significant effect on baseline $EPSC_1$ amplitudes (Fig. 2 *K–M*), suggesting tight coupling for SVs participating in tonic release. Most strikingly, however, EGTA-AM completely blocked the potentiation of $EPSC_1$ amplitudes when applied before baclofen (Fig. 2 *K–M*), suggesting that the induction of phasic release strongly depends on Ca^{2+} distant from Cav2.3. Furthermore, Ca^{2+} imaging of MHb axons confirmed a significant reduction in stimulation-induced GCaMP6s fluorescence after EGTA-AM application. Bath application of baclofen restored GCaMP6s fluorescence to baseline levels but not beyond (Fig. 2 *N* and *O*). These results support our hypothesis that diffusion of Ca^{2+} away from Ca^{2+} channels recruits loosely coupled SVs to the RRP during phasic release induction.

In summary, our results suggest that 1) Ca^{2+} increase induced by activation of GBRs in MHb terminals is necessary for the recruitment of SVs from distal sites of the terminal inducing phasic release; 2) increasing Ca^{2+} influx alone is insufficient to induce phasic release; and 3) SVs participating in phasic release are more loosely coupled to Cav2.3 than those participating in tonic release, indicating distinct release sites for these additional SVs.

Comparison of Release Properties of Tonic and Phasic Neurotransmission. We next compared RRP and P_r of basal and GBR-enhanced release by applying 30 stimulations at 100 Hz (Fig. 2 *P* and *Q*). Experiments were performed in the presence of 1 mM kynurenic acid to reduce saturation and desensitization of AMPA receptors. Although the use of back-extrapolating linear regression analysis may not be ideal for facilitating synapses (34), the 100-Hz stimulation did deplete baseline responses, allowing a rough estimation of the tonic RRP in cumulative EPSC amplitude plots (35). Strikingly, the application of baclofen increased the RRP on average 4.1-fold (Fig. 2*R*; baseline RRP: 0.58 ± 0.09 nA; baclofen RRP: 2.37 ± 0.36 nA; n = 16 cells, 4 mice). In addition, baclofen also increased P_r on average 2.0-fold (Fig. 2*S*; baseline: 0.086 ± 0.017; baclofen: 0.169 ± 0.024). Altogether, our results suggest that tonic and phasic release modes have different sizes of RRP with distinct coupling tightness.

Structural Correlates of Enhanced Neurotransmitter Release. The RRP is an electrophysiological property considered to be structurally reflected by docked SVs in the AZ (36, 37). To test

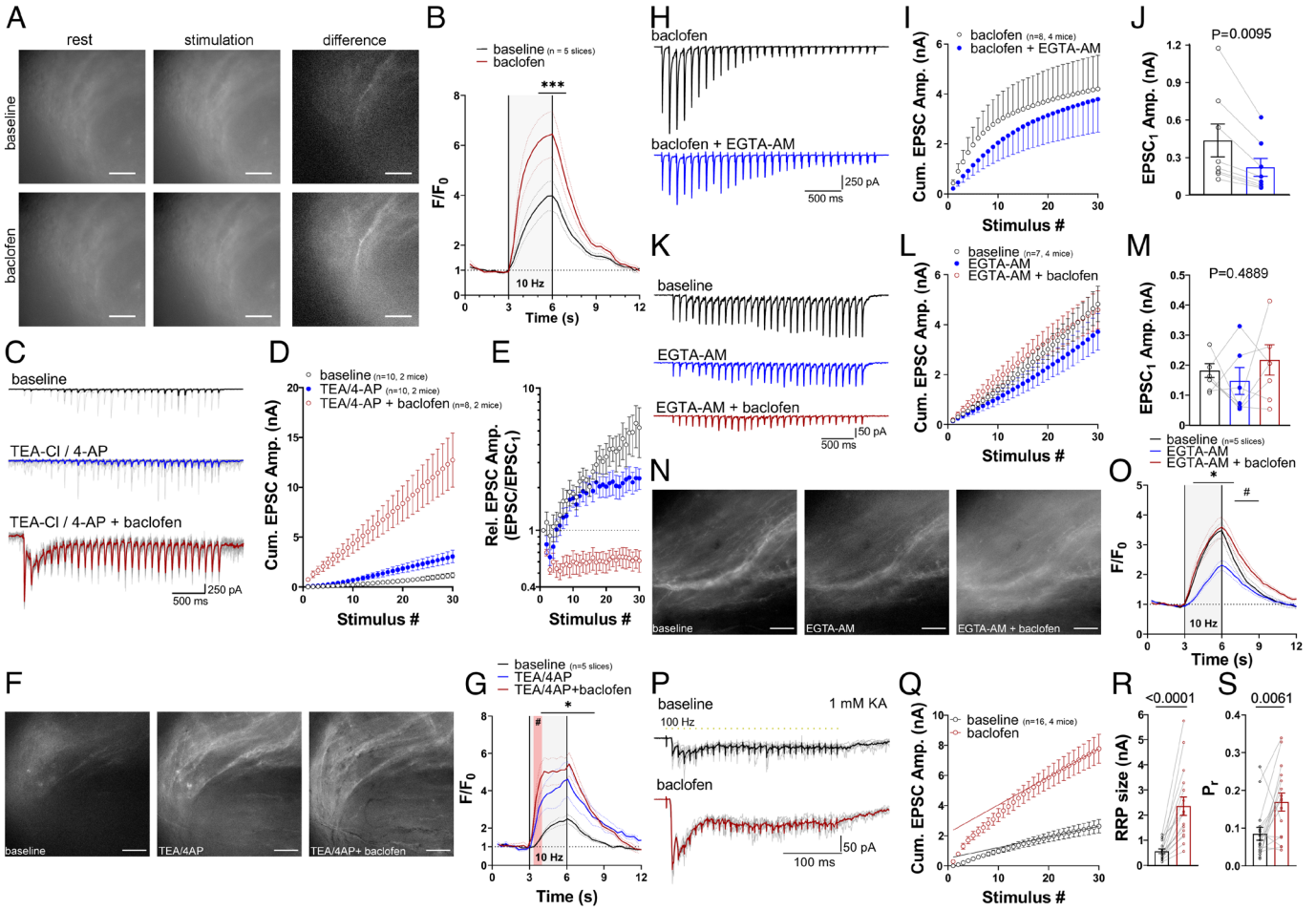

Fig. 2. Role of presynaptic Ca^{2+} in tonic and phasic neurotransmission. (*A*) Example images of axon-GCaMP6s fluorescence at rest (*Left*) and at peak fluorescence during stimulation (*Middle*) under baseline (*Top*) and baclofen conditions (*Bottom*). Subtraction of resting fluorescence from peak fluorescence reveals stimulation-induced fluorescence increase in a subset of MHb axons (*Right*). (Scale bars, 50 μm.) (*B*) Time course of GCaMP6s fluorescence change during stimulation under baseline and baclofen conditions in five slices from five mice. ***$P < 0.001$ two-way ANOVA with Bonferroni post hoc test; main effect of baclofen: $F_{(1, 328)} = 86.01$, $P < 0.0001$. (*C–E*) K^+ channel blockers TEA and 4-AP did not induce phasic release and did not occlude phasic release induction by baclofen. Notice the increase in spontaneous EPSCs in the example traces (*C*) of TEA/4-AP and TEA/4-AP+baclofen groups before and after 10-Hz stimulation. (*F*) The same as in *A*, at baseline (*Left*), the application of TEA/4-AP (*Middle*) and TEA/4-AP + baclofen (*Right*). (Scale bars, 50 μm.) (*G*) The time course of GCaMP6s fluorescence change reveals a significant increase in fluorescence by TEA/4-AP and TEA/4-AP + baclofen compared to baseline. TEA/4-AP and TEA/4-AP + baclofen groups only differed at the rising phase (red highlighted section) but not during peak fluorescence (Two-way ANOVA main factor of drug treatment: $F_{(2, 456)} = 107.4$, $P < 0.0001$; Tukey post hoc test: # indicates $P < 0.05$ between TEA/4-AP vs. TEA/4-AP + baclofen; * indicates $P < 0.05$ between baseline vs. TEA/4-AP and TEA/4-AP + baclofen). (*H*) Example trace of a phasic response before and 10 min after the application of 100 μM EGTA-AM. (*I*) Cumulative EPSC amplitude plot before and after EGTA-AM application. (*J*) Phasic $EPSC_1$ amplitude was significantly reduced by EGTA-AM. $P = 0.0095$, calculated with the paired *t* test. (*K–M*) Application of EGTA-AM prior to baclofen prevents phasic release induction but does not significantly alter tonic $EPSC_1$ amplitudes. Repeated measures one-way ANOVA: $F_{(1.902, 11.41)} = 0.7478$, $P = 0.4889$. (*N*) The same as in *A*, at baseline (*Left*), 15 min after the application of 100 μM EGTA-AM (*Middle*) and during the application of EGTA-AM + baclofen (*Right*). (Scale bars, 50 μm.) (*O*) EGTA-AM significantly reduced GCaMP peak fluorescence compared to baseline (Two-way ANOVA main effect of treatment: $F_{(2, 492)} = 162.6$, $P < 0.0001$; * indicates $P < 0.05$ EGTA-AM vs. baseline and EGTA-AM + baclofen groups, Tukey post hoc test), whereas the addition of baclofen restored GCaMP peak fluorescence to baseline levels, but fluorescence decayed slower than baseline. # indicates $P < 0.05$ between EGTA-AM + baclofen vs. baseline and EGTA-AM, Tukey post hoc test. (*P*) Example traces of EPSC responses during 100-Hz stimulation at baseline and after baclofen application. (*Q*) Baseline and baclofen cumulative EPSC amplitude plots with linear regression fit through the last 6 stimuli (#25 to #30). (*R*) Paired comparison of RRP sizes before and after baclofen. $P < 0.0001$, Wilcoxon test. (*S*) Paired comparison of P_r at baseline and after baclofen, $P = 0.0061$ calculated by the two-tailed paired *t* test. See also *SI Appendix*, Fig. S3 and Table S1.

this, we performed timed high-pressure freezing after optogenetic stimulation of MHb terminals in acute slices [*SI Appendix*, Fig. S4*A*, Flash and Freeze (18)]. First, we measured optogenetic responses in IPN neurons of ChAT-ChR2-EYFP mice (20) in 200-μm-thick coronal slices (Fig. 3*A*). In ChAT-ChR2-EYFP mice, 90.2% of asymmetrical synapses expressed channelrhodopsin2 in the rostral/central IPN region (*SI Appendix*, Fig. S4*B*). Under baseline conditions, optogenetic stimulation at 10 Hz produced tonic-like EPSC responses that decayed over time after the 10-Hz train (Fig. 3 *A* and *B*). However, in contrast to electrically evoked EPSCs, optogenetically evoked $EPSC_1$ amplitudes were frequently larger than subsequent EPSCs. This likely resulted from the desensitizing kinetics of channelrhodopsin, exhibiting an initially larger conductance than during repetitive activity (38, 39), and larger number of stimulated axons with optogenetic than electrical stimulation. Stronger and broader optogenetic responses may also be explained by the Ca^{2+} conductance through ChR2 channels, the spillover of glutamate due to activation of most, if not all, cholinergic terminals, and the higher cholinergic tone in ChAT-ChR2-EYFP mice (40). Importantly, the application of baclofen-induced phasic release, which rapidly depleted during the 10-Hz train and recovered within 10 s (Fig. 3 *A* and *B*).

To examine the structural correlate of the GBR-induced increase in RRP size during phasic release induction, we chose to freeze MHb terminals at two time points in the presence of baclofen: 1) 100 ms after the 10-Hz stimulation (depletion group)

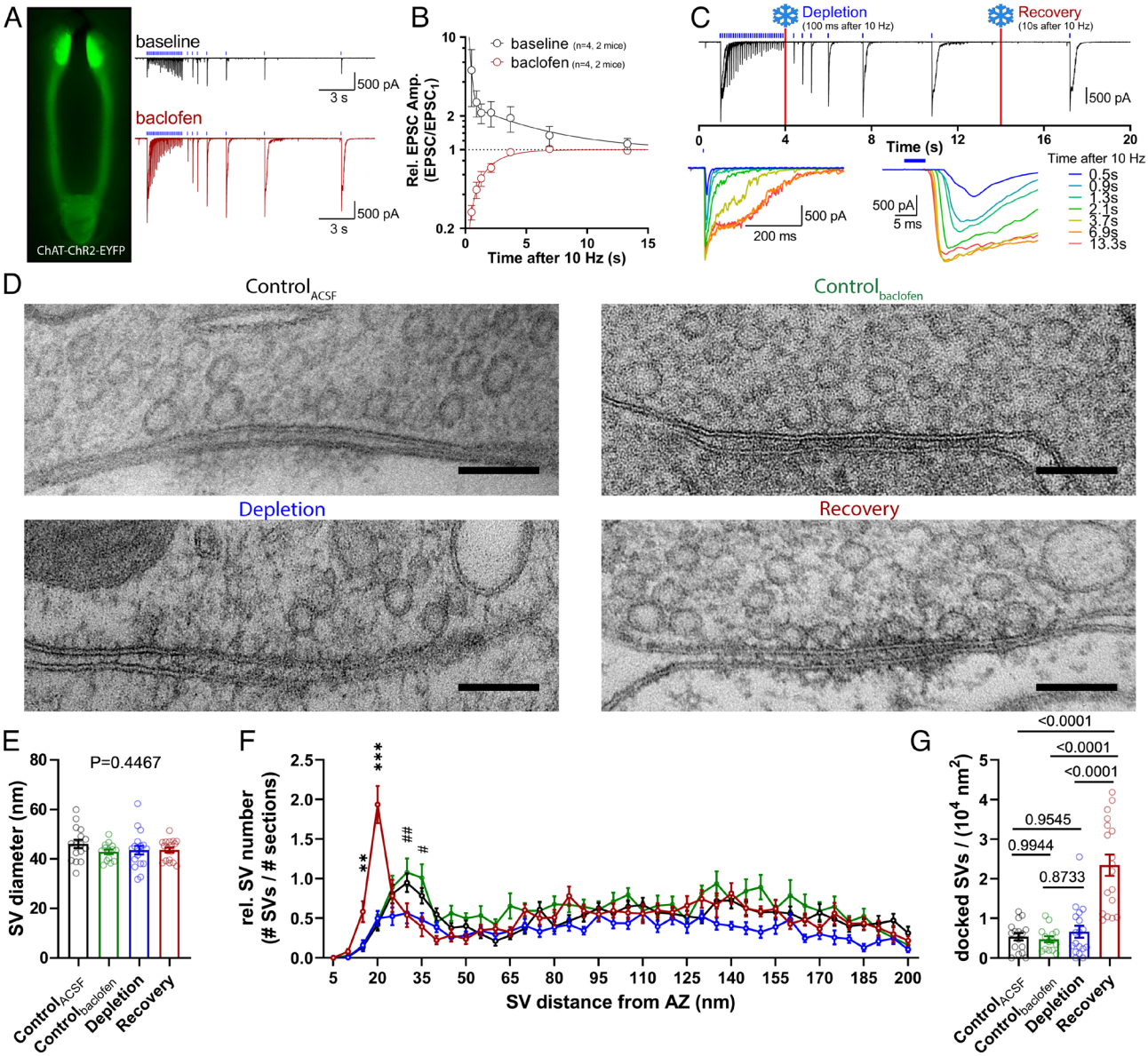

Fig. 3. Structural correlates of enhanced neurotransmitter release. (*A*) EYFP fluorescence in an angled ChAT-ChR2-EYFP slice (*Left*) and tonic and phasic example traces evoked by optogenetic stimulation in a cell before and during the application of baclofen. (*B*) Recovery time courses of normalized EPSC amplitudes after augmentation (baseline) and depletion (baclofen). (*C*, *Top*) expanded phasic example trace from panel *A* highlighting freezing time points for depletion and recovery groups in the presence of baclofen. (*Bottom Left*) overlay of individual EPSCs over the course of recovery. (*Bottom Right*) overlay of individual EPSC onsets during phasic release recovery. (*D*) Example electron micrographs of synapses from $Control_{ACSF}$, $Control_{baclofen}$, Depletion, and Recovery groups. (Scale bars, 100 nm.) (*E*) Quantification of SV diameters across groups. *P* value derived from one-way ANOVA. $F_{(3, 62)} = 0.8994$, $P = 0.4467$. (*F*) Plot of SV numbers (normalized to the number of analyzed serial sections) in distance bins of 5 nm from the SV center to the nearest AZ membrane. ***$P < 0.001$, **$P < 0.01$ Recovery vs. Controls and Depletion, ##$P < 0.01$, #$P < 0.05$ Controls vs. Recovery and Depletion, two-way ANOVA with Tukey post hoc test. Main group effect: $F_{(3, 2480)} = 49.12$. $P < 0.0001$. (*G*) Quantification of docked SV densities in serial sections. Values above bars indicate *P* values calculated by one-way ANOVA with the Tukey post hoc test. $F_{(3, 62)} = 26.66$, $P < 0.0001$. See also *SI Appendix*, Fig. S4.

at which time point the phasic RRP should be mostly depleted, and 2) 10 s after the 10-Hz stimulation (recovery group) at which time point the phasic RRP should have fully recovered (Fig. 3*C* and *SI Appendix*, Fig. S4*A*). We tested two different control conditions: $Control_{ACSF}$ and $Control_{baclofen}$ samples were high-pressure frozen in the same way as recovery and depletion samples but without light stimulation in the absence or presence of baclofen. Following freeze substitution, we extracted the rostral/central IPN region and prepared serial ultrathin sections (40 nm) for electron microscopy (EM) (*SI Appendix*, Fig. S4 *C* and *D* and Fig. 3*D*). SV diameters were not significantly different between groups ($Control_{ACSF}$: 46.0 ± 1.7 nm, n = 16 synapses, 3 mice; 2,215 SVs measured; $Control_{baclofen}$: 42.9 ± 1.0 nm, n = 14 synapses, 2 mice, 1,535 SVs measured; Depletion: 43.4 ± 1.7 nm, n = 18 synapses, 3 mice, 2,204 SVs measured; Recovery: 43.6 ± 0.9 nm, n = 18 synapses, 3 mice, 2,539 SVs measured; Fig. 3*E*). In a defined perimeter around the AZ (*Methods*), we measured the distance from each SV's center to the nearest presynaptic membrane in 5-nm bins. SVs in direct contact with the presynaptic membrane or whose center was within 20 nm of the inner leaflet of the membrane were considered docked. In control samples, most SVs were in close proximity of the AZ but without making contact and, thus, considered as "loosely docked" (11) (20 - 40 nm distance from the AZ; 5th to 8th bins in Fig. 3*F*). The depletion group displayed lower numbers of SVs, particularly at the loosely docked bins. In contrast, the recovery group showed a significant

increase in docked SVs (first four bins in Fig. 3*F*). The density of docked SVs in the recovery group (2.34 ± 0.27 docked SVs/(10^4 nm^2); n = 18 terminals, 3 mice) increased 3.5-fold compared to the depletion group (0.67 ± 0.15 docked SVs/(10^4 nm^2); n = 18 terminals, 3 mice; Fig. 3*G*). The difference in docked SV densities between depletion and recovery groups was similar to that in RRP size between tonic and phasic release (4.1-fold, Fig. 2*R*). Interestingly, the density of docked SVs in $Control_{baclofen}$ group (0.47 ± 0.08 docked SVs/(10^4 nm^2) did not increase compared to the $Control_{ACSF}$ group, suggesting that GBR activation without presynaptic activity is insufficient to increase pool size.

SV-Associated Molecules Selectively Involved in Tonic and Phasic Release. We next aimed to identify proteins selectively involved in tonic and phasic release. We first investigated the role of SPO based on its selective expression in ventral MHb neurons (Allen Brain Atlas). SPO is a vesicular transmembrane protein of unknown function (41). In contrast to its homologue synaptophysin (42), SPO was found to coprecipitate with Cav2.3 in a brain-wide proteomics study (43), suggesting that it may be relevant for neurotransmission in MHb terminals which exclusively rely on Cav2.3 for release (8). Immunofluorescence revealed that SPO was expressed in axon-like structures in the rostral/central but not lateral IPN subnuclei (Fig. 4*A*). At the EM level, SPO-labeling was confirmed on SVs in MHb terminals (Fig. 4*B*, also see Fig. 4 *S*–*T*). We then generated SPO KO mice (*Methods*) and confirmed the specificity of immunolabeling (Fig. 4*A*). Whole-cell recordings from IPN neurons in SPO KO mice at baseline conditions (Fig. 4 *C*–*F*) revealed strongly impaired augmentation of tonic release (Fig. 4*D*). In contrast, baclofen-induced phasic release did not appear different from that of WT and P_r of $EPSC_1$ remained unaltered (Fig. 4 *E* and *F*; measured by linear regression analysis of cumulative EPSC amplitude plots). Recovery from phasic release depletion in SPO KO mice occurred with a similar time course (τ = 4.1 s, *SI Appendix*, Fig. S5 *A*–*C*) as in WT mice (τ = 4.4 s, Fig. 1*G*). These results suggest that SPO is a modulator of tonic release augmentation.

Phasic release, on the other hand, requires the cytosolic Ca^{2+}-dependent activator protein for secretion (CAPS) in the hippocampus (11, 44). Of the two CAPS isoforms, only CAPS1 is required for fast, phasic neurotransmission in the hippocampus (44), whereas CAPS2 is involved in the release of neuropeptides and neurotrophic factors (45, 46). Since MHb neurons exclusively express CAPS2 but not CAPS1 (47), we hypothesized that CAPS2 might be involved in GBR-induced phasic release. Immunofluorescence revealed strong CAPS2 expression in all IPN subnuclei (Fig. 4*G*) and pre-embedding EM showed CAPS2 labeling in MHb terminals in the rostral/central IPN (Fig. 4*H*). We then performed whole-cell recordings in IPN neurons of CAPS2 KO mice (44) (Fig. 4 *I*–*L*). Functionally, tonic release appeared intact, with augmentation similar to that of WT (Fig. 4 *I* and *J*). However, phasic release was strikingly altered (Fig. 4 *K* and *L*). Specifically, P_r of $EPSC_1$ was reduced almost 10-fold compared to WT (WT $EPSC_1$ P_r: 0.19 ± 0.02, n = 13 cells, 5 mice; CAPS2 KO $EPSC_1$ P_r: 0.02 ± 0.00, n = 14 cells, 3 mice, Fig. 4*L*). Furthermore, P_r increased over the first four stimuli before gradually reducing. Recovery from 10-Hz phasic release (*SI Appendix*, Fig. S5 *D*–*F*) consisted of an initial increase in EPSC amplitudes early after the 10-Hz stimulus (0.5 to 2.1 s post 10-Hz), followed by an exponential decay with a time constant of τ = 7.3 s (2.1 to 13.3 s post 10-Hz), which is similar to the recovery time course of augmentation in WT mice (τ = 6.9 s, Fig. 1*G*). This pattern may result from fast replenishment of depleted SVs at high residual Ca^{2+} concentrations within the first 2 s, followed by slowing of the replenishment rate at near resting Ca^{2+} concentrations. This result suggests that the augmentation observed in the absence of baclofen in WT still occurs during phasic release in the presence of baclofen but is masked by the prominent depression (21).

Interestingly, we observed a phasic response pattern in WT mice similar to that of CAPS2 KO mice, but only at the very first 10-Hz stimulation in the presence of baclofen (*SI Appendix*, Fig. S6 *A* and *B*). Therefore, these results suggest that CAPS2 is recruited Ca^{2+} dependently during phasic release induction and might serve to facilitate docking of replenished SVs. Nonetheless, the facilitation in the first several stimuli followed by depression in CAPS2 KO mice (Fig. 4*K*) indicates that CAPS2 does not interfere with the Ca^{2+}-dependent recruitment of phasic release SVs. Overall RRP size remained unaffected in CAPS2 KO compared to WT mice (*SI Appendix*, Fig. S6 *C*–*E*), but the release-competent subpool at rest is substantially smaller in CAPS2 KO mice.

We next examined whether SPO and CAPS2 are colocalized in the same MHb terminals. Double immunofluorescence showed a large overlap of labeling for CAPS2 with that for SPO in the rostral/central IPN (Fig. 4*M*). Double pre-embedding EM immunolabeling with small particles for SPO and large particles for CAPS2 revealed their colocalization in the same terminals (Fig. 4 *N* and *O*). In samples incubated with anti-SPO or anti-CAPS2 antibodies alone with the same double-labeling protocol, we mostly found small or large particles, respectively, indicating minimal cross-reactivity of the secondary antibodies (Fig. 4*P*). These samples allowed the quantification of SPO and CAPS2 particle sizes, which were reliably distinguishable (Fig. 4*Q*; SPO particle diameter: 5.85 ± 0.30 nm, n = 298 particles; CAPS2 particle diameter: 32.40 ± 0.50 nm, n = 452 particles). We then measured the distance from CAPS2 particles (diameter >14 nm) to the nearest SPO particle (diameter <8 nm) and compared these real NND values with those from simulated SPO to real CAPS2 particles (Fig. 4*R*). SPO to CAPS2 NNDs were not significantly different from those of random distributions generated using simulations. Importantly, CAPS2 is a cytosolic protein (44), and whether CAPS2 associates with SVs in MHb terminals is unclear. Therefore, we measured the distance from CAPS2 and SPO particles to the closest SV membrane in single immunolabeling samples (Fig. 4*S*). We found similar distributions relative to the SV membrane for SPO and CAPS2 (Fig. 4*T*) with a slightly but significantly shorter distance for SPO (3.49 ± 0.16 nm, n = 320 particles) than CAPS2 (4.73 ± 0.30 nm, n = 152 particles). This difference may be ascribable to larger diameter of CAPS2 particles (8.6 ± 3.2 nm, mean ± SD, n = 132 particles) than SPO particles (4.3 ± 2.5 nm, mean ± SD, n = 147 particles) (48). Overall, we identified SPO and CAPS2 as SV-associated proteins located inside the same presynaptic terminals and selectively involved in tonic and phasic release, respectively.

Impact of GBR Activation and CAPS2 KO on Quantal Size. We then asked whether quantal size was affected by either GBR activation or loss of CAPS2. To this aim, we measured miniature EPSC (mEPSC) frequency and amplitude before and during baclofen application in WT and CAPS2 KO mice (*SI Appendix*, Fig. S6 *F*–*H*). Interestingly, GBR activation did not affect mEPSC amplitudes in either genotype but significantly reduced mEPSC frequencies in WT and CAPS2 KO mice (*SI Appendix*, Fig. S6 *F* and *G*). The mEPSC frequency and amplitude at baseline or during baclofen application were not different between genotypes (*SI Appendix*, Fig. S6*H*). Next, we utilized the pronounced asynchronous release after single stimuli in the presence of baclofen to quantify quantal asynchronous EPSC (aEPSC) amplitudes (*SI Appendix*, Fig. S6 *I*–*K*) (49). We found no significant difference in aEPSC amplitudes between genotypes and no significant difference in amplitudes between aEPSC and

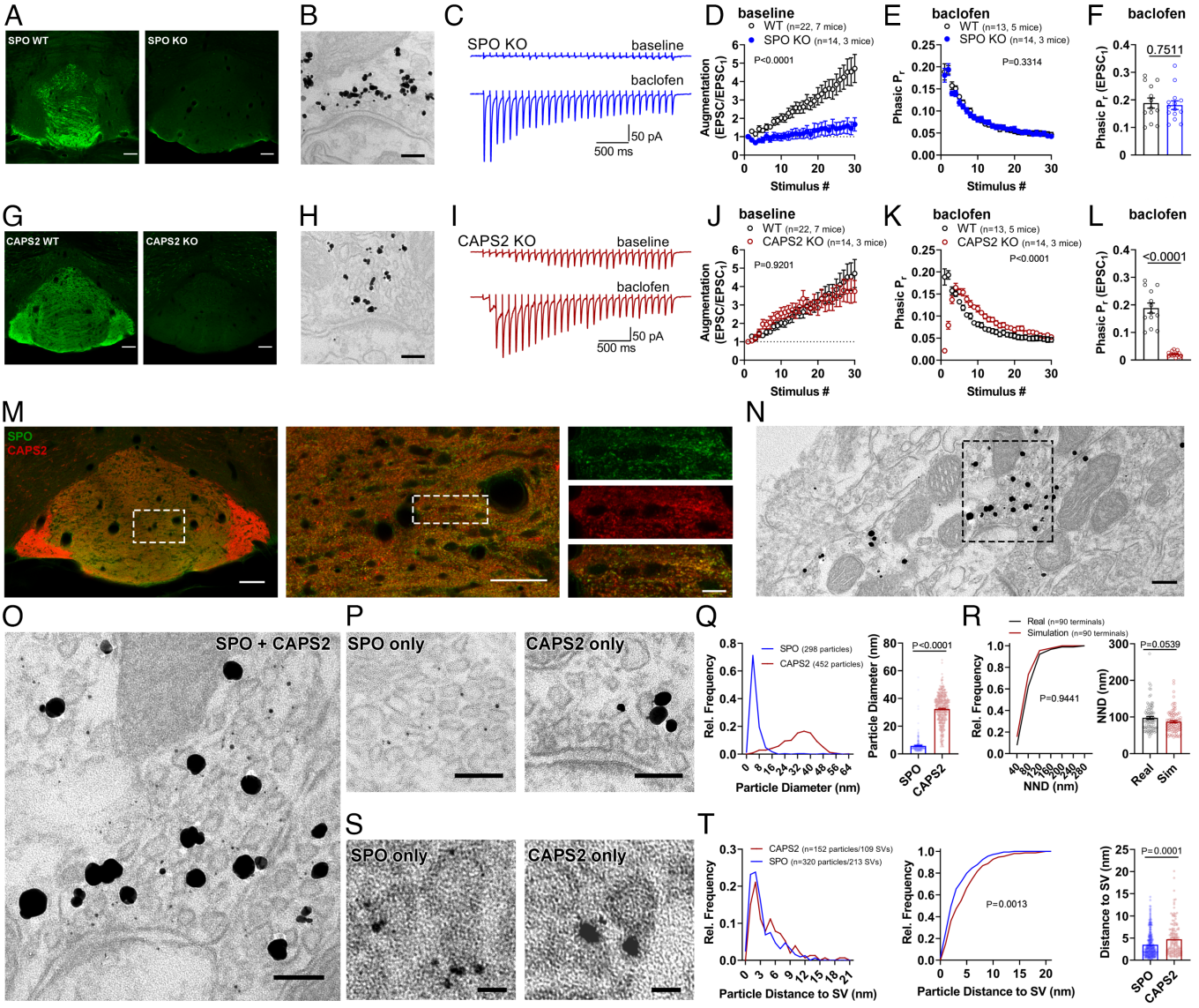

Fig. 4. SPO and CAPS2 involved in tonic and phasic neurotransmitter release are colocalized to the same terminals and vesicle-associated. (*A*) Confocal images of SPO immunofluorescence in the IPN of a WT and a SPO KO mouse. (Scale bars, 100 μm.) (*B*) Pre-embedding EM immunolabeling for SPO in an MHb terminal. (Scale bar, 100 nm.) (*C*) Example 10-Hz EPSC traces from a SPO KO mouse at baseline and during baclofen application. (*D*) Tonic release augmentation was significantly impaired in SPO KO mice. Main effect of genotype, calculated by two-way ANOVA: $F_{(1, 1020)} = 212.8$, $P < 0.0001$. Bonferroni post hoc analysis revealed a significant difference in stimuli #20 to #30. (*E*) Overlay of phasic release P_r time course between WT and SPO KO mice, calculated by linear regression analysis of cumulative EPSC amplitude plots (35). Main effect of genotype calculated by two-way ANOVA: $F_{(1, 750)} = 0.9445$, $P = 0.3314$. (*F*) P_r of $EPSC_1$ in the phasic response train was not different between WT and SPO KO mice. $P = 0.7511$ calculated from two-tailed unpaired *t* test. (*G*) Confocal images of anti-CAPS2 immunofluorescence in the IPN of a WT and CAPS2 KO mouse. (Scale bars, 100 μm.) (*H*) Pre-embedding immunolabeling for CAPS2 in a MHb terminal. (Scale bar, 100 nm.) (*I*) Example 10-Hz EPSC traces from a CAPS2 KO mouse at baseline and during baclofen application. (*J*) Augmentation remained unaffected by genetic ablation of CAPS2. Main effect of genotype calculated via two-way ANOVA: $F_{(1, 1020)} = 0.01006$, $P = 0.9201$. (*K*) P_r time course of phasic release, calculated by linear regression analysis of cumulative EPSC amplitude plots, was strongly affected by genetic ablation of CAPS2. Main effect of genotype calculated by two-way ANOVA: $F_{(1, 750)} = 22.73$, $P < 0.0001$. Bonferroni post hoc test revealed a significant difference at Stimuli #1, 2, 6, 7, 9, and 11. (*L*) P_r of $EPSC_1$ in the phasic response was significantly lower in CAPS2 KO compared to WT mice. $P < 0.0001$ calculated by two-tailed unpaired *t* test. (*M*, *Left*) double immunofluorescence for CAPS2 (red) and SPO (green), showing strong overlap in the rostral and central IPN. (*Middle*) higher magnification of the dashed square in the *Left* panel. (*Right*) higher magnification of the dashed square in the *Middle* panel. (Scale bars from *Left* to *Right*, 100 μm, 50 μm, and 10 μm.) (*N*) Example image of double pre-embedding EM immunolabeling for SPO and CAPS2 in the rostral/central IPN. (Scale bar, 200 nm.) (*O*) High magnification image of the dashed-line square in *N*. SPO and CAPS2 labeled by small and large particles, respectively. (Scale bar, 100 nm.) (*P*) Example images of single labeling for SPO (*Left*) and CAPS2 (*Right*) with the same double pre-embedding labeling protocol as for (*O* and *N*). (Scale bar, 100 nm.) (*Q*) Quantification of particle diameters for SPO and CAPS2 based on the single labeling in *P*. (*Left*) frequency distribution histogram shows minimal overlap of particle sizes. (*Right*) Average particle diameter for SPO (5.8 ± 0.3 nm) and CAPS2 (32.4 ± 0.5 nm). *P* value derived from Mann–Whitney test. (*R*) NND from CAPS2 to SPO particles in double pre-embedding labeling. NND of real CAPS2 (>14 nm) to SPO particles (<8 nm) was not different from that of random simulation. *P* values derived from Kolmogorov–Smirnov test (*Left*) and Mann–Whitney test (*Right*). (*S*) High magnification image of single labeling for SPO (*Left*) and CAPS2 (*Right*) with short silver intensification to produce small particles. (Scale bar, 20 nm.) (*T*) Frequency histogram of SPO and CAPS2 particle distance to the center of the SV membrane (*Left*), cumulative frequency histogram (*Middle*), and average distance between particles and SVs (*Right*). The average distances were 3.5 ± 0.2 nm for SPO and 4.7 ± 0.3 nm for CAPS2. *P* values derived from Kolmogorov–Smirnov test (*Middle*) and Mann–Whitney test (*Right*). See also *SI Appendix*, Figs. S5 and S6.

mEPSC in the presence of baclofen (*SI Appendix*, Fig. S6*K*). These results suggest that quantal size remains unaffected by GBR activation or the loss of CAPS2. The reduction in mEPSC frequency by baclofen further suggests that GBR activation may exert distinct effects on spontaneous and evoked neurotransmitter release from MHb terminals.

Activity-Dependent Induction and Retention of Phasic Release. Our results suggest that prior activity may be necessary for recruiting new SVs to the RRP (*SI Appendix*, Fig. S6*A*) and that CAPS2 is required for the retention of these SVs (*SI Appendix*, Fig. S6*B*). Furthermore, GBR activation alone failed to increase the density of docked SVs in Flash and Freeze experiments (Fig. 3*G*). Therefore, we tested whether achieving the maximal phasic response is activity-dependent or whether GBR activation without activity is sufficient to reach peak potentiation. To this aim, we recorded bilateral MHb inputs to single IPN neurons and, after establishing a baseline response, stopped stimulation on one hemisphere while washing in baclofen (silent washin, Fig. 5 *A* and *B*). Once the 10-Hz stimulation (3 s, every 20 s) on the other hemisphere induced maximal potentiation, the same 10-Hz stimulation of the silent side resumed (Fig. 5*B*). Strikingly, $EPSC_1$ amplitude in the first 10-Hz stimulation train was only marginally increased, whereas the second train exhibited maximal potentiation of $EPSC_1$ amplitude. This result confirmed that the induction of phasic release is activity-dependent.

Next, we asked whether the GBR-mediated potentiation, once induced, might be stored in the absence of GBR activation and synaptic activity. To test this, we stimulated MHb inputs bilaterally to induce phasic release on both sides in the presence of baclofen. Once full potentiation was achieved, stimulation on one hemisphere was halted (silent washout) while starting the washout of baclofen (Fig. 5*C*). Five minutes after the washout onset, potentiation on the continuously stimulated side was fully reverted (stimulated washout). At this time point, we restarted the 10-Hz stimulation of the silent side and saw only marginal potentiation of $EPSC_1$ amplitudes in the first train ($EPSC_1$: 213.2 ± 62.3% of baseline amplitude, n = 9 cells, 4 mice; Fig. 5*C*). However, in the second train, $EPSC_1$ amplitudes increased to 46.8% of the peak potentiation (second train $EPSC_1$: 374.7 ± 82.8% of baseline amplitude; peak potentiation $EPSC_1$: 801.6 ± 120.4% of baseline amplitude). Therefore, we conclude that the GBR-mediated potentiation can be stored for minutes in the absence of GBR activation, but the retrieval of this stored potentiation requires activity, consistent with the idea of activity-dependent recruitment of additional docked SVs (Fig. 3*G*).

Translocation of CAPS2 to the Presynaptic AZ by Phasic But Not Tonic Release. Given the partial storage of GBR-mediated potentiation for at least 5 min (Fig. 5*C*), we hypothesized that chemical fixation might be sufficiently fast to capture molecular changes underlying the phasic release induction. Therefore, we combined optogenetic stimulation of MHb terminals in acute IPN slices from ChAT-ChR2-EYFP mice and immersion chemical fixation followed by pre-embedding immunolabeling of CAPS2 and SPO ("Flash and Fix"). Control slices remained unstimulated and unexposed to baclofen, whereas the "10 Hz" group received three 10-Hz light stimulations (3-s duration, 10-s interval) without baclofen, and the "10 Hz + Baclofen" group received the same stimulation after a 10 to 15 min preincubation in 1 µM baclofen. Immediately after the last stimulation, slices were submerged in a fixative [4% paraformaldehyde (PFA), 0.05% glutaraldehyde, 15% picric acid] for 45 min. Pre-embedding immunolabeling revealed that CAPS2 but not SPO was specifically recruited to the presynaptic AZ in the 10 Hz + Baclofen group (Fig. 6 *A*–*D*; CAPS2 Control: 0.3 ± 0.1 particles/AZ, n = 58 profiles, 2 mice; 10 Hz: 0.7 ± 0.1 particles/AZ, n = 68 profiles, 2 mice; 10 Hz + Baclofen: 2.6 ± 0.3 particles/AZ, n = 60 profiles, 2 mice; SPO Control: 0.1 ± 0.0 particles/AZ, n = 80 profiles, 2 mice; 10 Hz: 0.2 ± 0.0 particles/AZ, n = 76 profiles, 2 mice; 10 Hz + Baclofen: 0.1 ± 0.0 particles/AZ, n = 88 profiles, 2 mice). Importantly, there was no AZ-translocation of CAPS2 after 10 to 15 min baclofen incubation without optogenetic stimulation (*SI Appendix*, Fig. S7 *A* and *B*; CAPS2 Control: 0.7 ± 0.1 particles/AZ, n = 75 profiles, 2 mice; Baclofen without stimulation: 0.6 ± 0.1 particles/AZ, n = 60 profiles, 2 mice). These results suggest an activity-dependent CAPS2 recruitment and subsequent stabilization in the presynaptic AZ during phasic, but not tonic release.

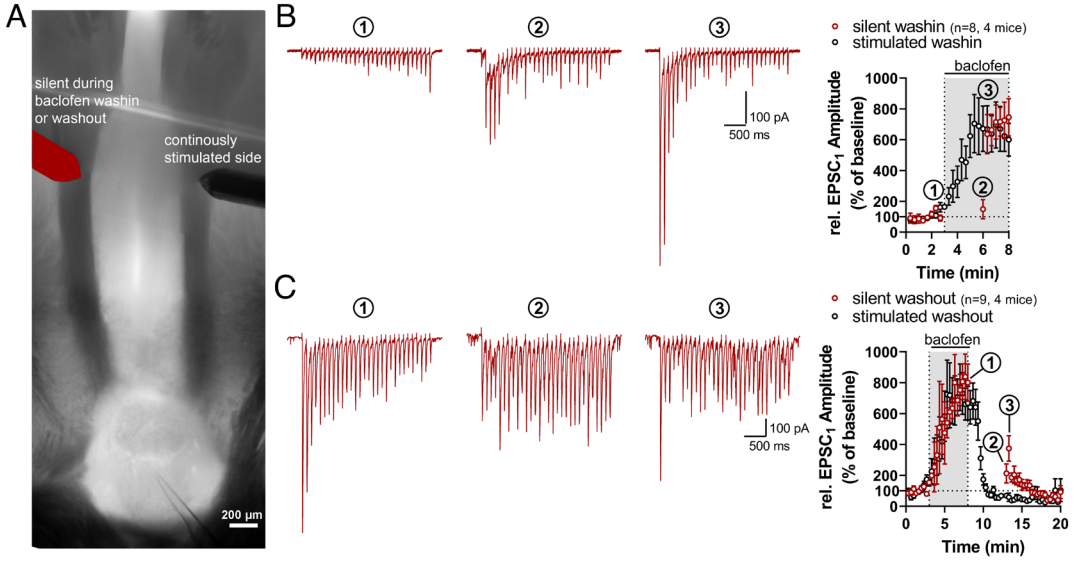

Fig. 5. Potentiation by GBR activation and its storage are activity-dependent. (*A*) Example thick-slice configuration of recording in IPN with bilateral MHb input stimulation. To examine activity dependence (*B*), a single IPN neuron was patched and after bilateral baseline recordings (10-Hz stimulation for 3 s, 5-s interval between *Left* and *Right* side stimulations, 20 s between sweeps), stimulation with the red-highlighted electrode was halted during baclofen washin, whereas stimulation was continued with the other electrode (10 Hz, 3-s duration, every 20 s). Once maximal potentiation was reached, stimulation with the red-highlighted electrode resumed. To examine storage of potentiation (*C*), after bilateral baseline recording and bilateral induction of maximal potentiation, baclofen washout commenced and stimulation with the red-highlighted electrode was halted. Stimulation with the other electrode continued and, once potentiation was fully reverted, stimulation with the red-highlighted electrode resumed. (*B*, *Left*) example traces derived from the silent side at baseline (1), at the first (2) and second (3) 10-Hz stimulus after silent baclofen washin. (*Right*) time course of $EPSC_1$ amplitudes, relative to baseline, during stimulated and silent washin of baclofen. (*C*, *Left*) example traces derived from the silent side at peak potentiation (1), at the first (2) and second (3) stimulus after silent baclofen washout. (*Right*) time course of relative $EPSC_1$ amplitudes during stimulated and silent washout of baclofen.

Flash and Freeze-Fracture Directly Reveals Selective Recruitment of CAPS2 to the Presynaptic Membrane during Phasic Release. Is CAPS2 rapidly recruited to the AZ selectively during the induction of phasic release or does CAPS2 also participate in tonic release but without prolonged retention in the AZ? Furthermore, is AZ-located CAPS2 in "Flash and Fix" experiments inserted in the membrane or localized to SV membranes close to the AZ? To answer these questions, we combined Flash and Freeze with freeze-fracture replication and subsequent immunolabeling. This method, which we termed Flash and Freeze-fracture, enables the nanoscale detection of multiple proteins simultaneously in the presynaptic membrane within milliseconds of neurotransmitter release (Fig. 6*E*).

If CAPS2 is selectively recruited during phasic release, the ratio of CAPS2 to SPO molecules in the presynaptic membrane should shift toward CAPS2 compared to tonic release. To test this prediction, we quantified the ratio of CAPS2 to SPO in the presynaptic membrane following stimulation by a single 8-ms light pulse in the absence or presence of baclofen. Since phasic SV recruitment is activity-dependent (*SI Appendix*, Fig. S6*A* and Fig. 5*B*), two 10-Hz conditioning stimuli (3-s duration, 10-s interval) were given 10 s prior to the single light pulse. Freezing was timed so that the tissue reached 0 °C 8 ms after light onset and light application continued for an additional 15 ms during freezing. To maximize transmitter release and stabilize SV- and membrane-associated proteins in the presynaptic membrane after fusion, slices were stimulated and frozen in the presence of 1 mM

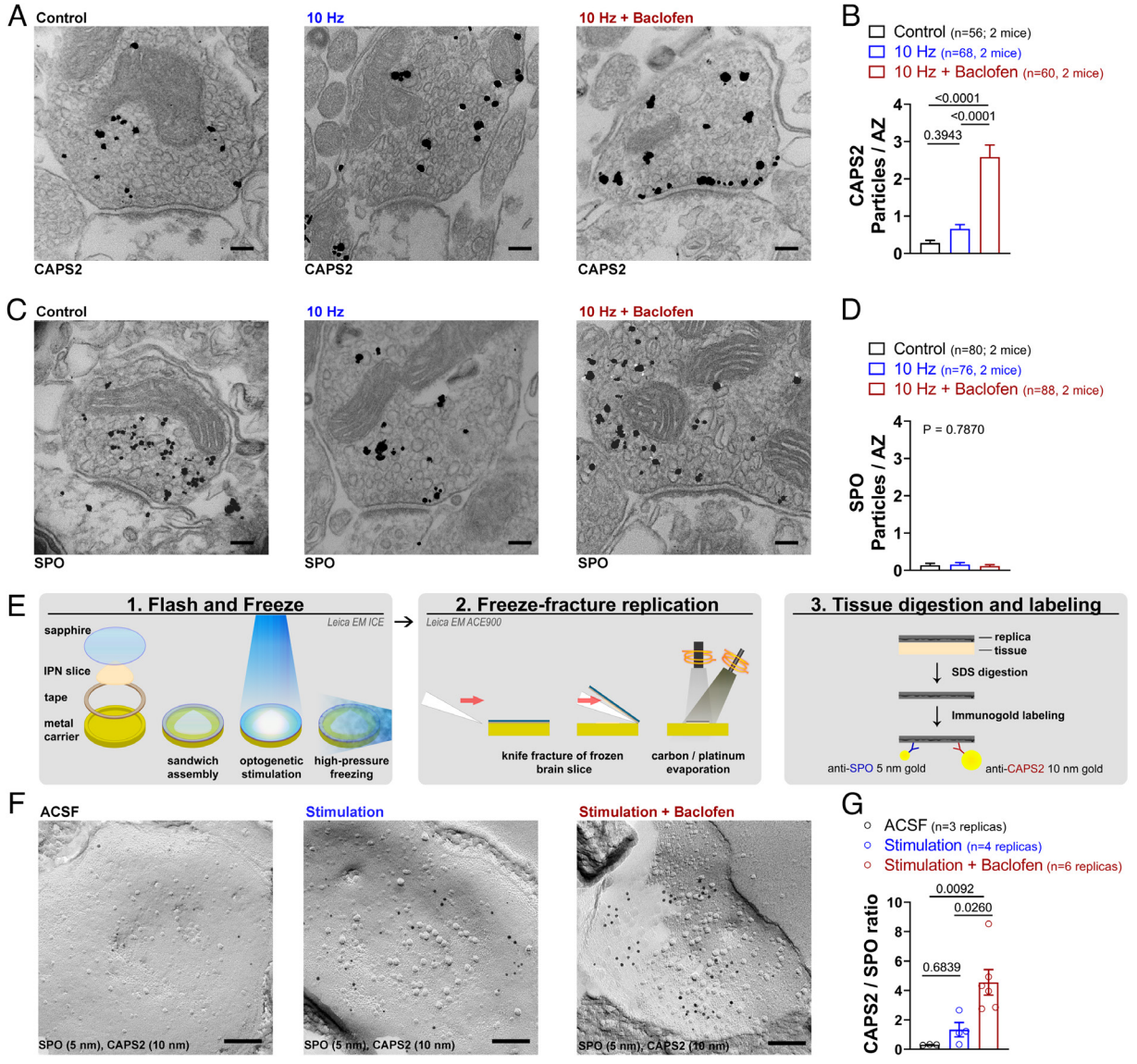

Fig. 6. Selective recruitment of CAPS2 to the AZ after GBR activation. (*A*) Example images of pre-embedding EM labeling for CAPS2 in acute slices under control conditions without stimulation and after 10-Hz stimulation in the absence (10 Hz) or presence of 1 μM baclofen (10 Hz + Baclofen). (Scale bars, 100 nm.) (*B*) Quantification of the number of particles touching the presynaptic membrane in the AZ reveals significantly higher CAPS2 numbers in the "10 Hz + Baclofen" group compared to the other groups. *P* values calculated by one-way ANOVA with Tukey post hoc test: $F_{(2, 178)} = 35.69$, $P < 0.0001$. (*C*) The same as in *A* for SPO. (Scale bars, 100 nm.) (*D*) The same as in *B* for SPO, showing no difference between groups. *P* values calculated by one-way ANOVA: $F_{(2, 241)} = 0.2397$, $P = 0.7870$. (*E*) Flash and Freeze-fracture steps schematic. (*Left*) Flash and Freeze of acute brain slices using a sapphire/metal hybrid sandwich separated by a double-sided tape. (*Middle*) Freeze-fracture replication of frozen brain slices using a knife to separate the sapphire disc from the metal carrier. (*Right*) SDS treatment of tissue and immunolabeling with primary antibodies against SPO and CAPS2 followed by labeling with 5 nm and 10 nm gold-conjugated secondary antibodies. (*F*) Example images of SPO and CAPS2 labeling in Flash and Freeze-fracture replicas frozen without light stimulation (ACSF) or after an 8-ms light pulse in the absence (Stimulation) or presence of 1 μM baclofen (Stimulation + Baclofen). (Scale bars, 100 nm.) (*G*) Quantification of CAPS2/SPO particle ratio in the AZ membrane revealed a significant increase in the "Stimulation + Baclofen" group. *P* values derived from one-way ANOVA with Tukey post hoc test $F_{(2, 10)} = 8.930$, $P = 0.0060$. See also *SI Appendix*, Figs. S7 and S8.

TEA-Cl, 100 μM 4-AP and 100 μM of the dynamin inhibitor dynasore. Because CAPS2 is a cytosolic protein, we incubated replicas with attached tissue in 2% PFA for 1 h prior to sodium dodecyl sulfate (SDS) digestion to cross-link CAPS2 to potential interacting transmembrane proteins. In Flash and Freeze-fracture replicas of the "Stimulation + Baclofen" group, the ratio of CAPS2 to SPO (4.56 ± 0.87, n = 6 replicas, 205 profiles, 6 mice) was significantly higher than in the unstimulated control group (ACSF, 0.31 ± 0.01, n = 3 replicas, 153 profiles, 3 mice) and "Stimulation" group (1.33 ± 0.48, n = 4 replicas, 320 profiles, 4 mice; Fig. 6 *F* and *G*). We confirmed the specificity of replica labeling for SPO and CAPS2 in acute-slice replicas of corresponding KO mice (*SI Appendix*, Fig. S8*A*). The difference in the ratio during phasic release (Fig. 6*F*) derived from increases in the density of CAPS2 in the presynaptic membrane as SPO density was similar across all three groups (*SI Appendix*, Fig. S8*B*), potentially due to high spontaneous neurotransmission in the presence of TEA + 4-AP (Fig. 2*C*). Comparison of SPO and CAPS2 particle numbers in individual AZs revealed a significant positive correlation in the stimulation + baclofen group but not in the stimulation group (*SI Appendix*, Fig. S8*C*), indicating that baclofen induced the CAPS2 translocation accompanied with evoked vesicular release. Finally, to test the association between SPO and CAPS2 in the AZ, we compared the NNDs from CAPS2 to SPO particles with those from real CAPS2 to simulated SPO particles (*Methods*). Interestingly, NND analysis revealed no significant association between CAPS2 and SPO in the presynaptic membrane of both stimulation and stimulation + baclofen groups (*SI Appendix*, Fig. S8*D*), suggesting that CAPS2-binding and SPO-associated vesicle fusion sites may not overlap.

Discussion

Our results shed light on the mechanisms of GBR-mediated potentiation of MHb-IPN synapses. Although the signaling pathways downstream of GBR activation remain elusive, our experiments show that 1) the GBR-mediated potentiation involves a transition from a tonic to a phasic release mode, 2) the transition is associated with an increase in both functional (RRP) and structural (docked SVs) pool size, 3) SVs mediating phasic release are more loosely coupled to presynaptic Ca^{2+} channels than those mediating tonic release, 4) induction of potentiation is activity-dependent, 5) noncanonical signaling, such as cAMP-PKA and PKC pathways, is not involved in the potentiation, 6) CAPS2 translocates to the presynaptic AZ selectively during phasic release and retains the RRP increase for several minutes, and 7) SPO is selectively involved in augmentation during tonic release.

Tonic and phasic release are generally thought to be synapse-specific properties, widely used as hallmarks for synaptic identification (12). However, our results demonstrate that GBR activation converts the same synapse from a tonic into a phasic release mode. One possibility is that different populations of vesicles, for example with different Ca^{2+} sensitivity, mediate tonic and phasic responses (50). The heterogeneity of the vesicle pool has emerged with a diverse array of molecules (51). The selective increase of CAPS2 at the AZ during phasic release may indicate a distinct SV pool involved in the potentiation, separate from the SPO-associated SVs used in the baseline condition.

Alternatively, a recently proposed sequential priming model of a homogenous SV pool (19) may explain our results. Under baseline conditions, the majority of SVs may be in a loosely docked state (LS) with only a small proportion of SVs in a tightly docked, fusion-competent state (TS, Control in Fig. 3*D*). With repeated stimulation in the presence of baclofen, SVs may gradually transition Ca^{2+} dependently from LS to TS, shifting the ratio of LS/TS pools toward TS (Recovery in Fig. 3*D*). The distance distribution of SVs from the plasma membrane would be consistent with this model (Fig. 3*F*). Furthermore, the experimental observation that tonic release in the absence of baclofen and phasic release in its presence converge toward a common steady-state value (Fig. 1*D*) is predicted by the model. The release pattern of the loosely docked pool model closely matches our bimodal phasic release pattern (facilitation to depression) in the first repetitive stimulation in WT and all repetitive stimulations in CAPS2 KO mice after GBR activation, indicating that CAPS2 may retain the TS pool required for the release pattern of the tightly docked pool model.

Interestingly, baclofen increased stimulation-evoked release but decreased the frequency of miniature release (*SI Appendix*, Fig. S6 *F–H*). Given that 90% of terminals in the rostral/central IPN originate from cholinergic MHb neurons (*SI Appendix*, Fig. S4*B*), it is unlikely that baseline mEPSCs derived from other excitatory projections that exhibit GBR-mediated presynaptic inhibition. Thus, GBRs may differentially regulate evoked and spontaneous neurotransmission, potentially due to distinct Ca^{2+} dependencies (7). Alternatively, spontaneous and evoked release may arise from distinct release sites that are differentially affected by GBR signaling (52).

The present results also shed light on the function of two synaptic proteins with largely unknown function, SPO and CAPS. SPO is highly expressed in the MHb, and tightly coupled to Cav2.3 R-type Ca^{2+} channels (43). Cav2.3 may serve as an anchor point for tonic SVs during augmentation and loss of binding to this anchor in the SPO KO mice might result in impaired recruitment of tonic SVs to the AZ during tonic release. Alternatively, SPO may stabilize v-SNAREs as recently reported for its homologue Synaptophysin (53).

CAPS2 is also abundantly expressed in the MHb terminals, which exclusively express this isoform (47). Although CAPS2 is not essential for the GBR-mediated potentiation, it markedly regulates kinetic properties of phasic release (Fig. 4 *I–L*), stabilizing the GBR-mediated SV pool increase for minutes. The mechanisms of this regulation and its recruitment to the AZ during phasic release remain to be clarified. The positive correlation between CAPS2 and SPO numbers in each AZ only in the presence of baclofen supports the idea that the recruitment of CAPS2 to the AZ during phasic activity could result from the fusion of CAPS2-associated SVs in stimulated terminals, although cytosolic CAPS2 may also be recruited to the AZ by other mechanisms, potentially via the Ca^{2+} binding C2 and the pleckstrin homology domains (54). CAPS2 remaining at the AZ might serve as docking sites for replenished SVs via MUN domains (54), which has sequence homology to the priming protein Munc13. In this scenario, it could also be involved in SV priming (44) and may contribute to the transient nature of the GBR-mediated potentiation. Another study found that CAPS2-mediated RRP recruitment requires the pleckstrin homology but not the MUN domain, suggesting that PIP_2 binding might be important (55). However, PLCη2 KO mice showed no alteration in GBR-mediated potentiation, despite a previous report of negative regulation of CAPS by this PLC isoform (27). No involvement of other PLC/PKC pathway components suggests that the PIP_2-binding activity of CAPS2 may not be required for the activity-dependent AZ-translocation of CAPS2 during phasic release induction.

Activity dependence of the baclofen effect (Fig. 5) suggests that presynaptic GBRs in MHb-IPN terminals may implement a new form of short-term heterosynaptic plasticity between glutamatergic-cholinergic MHb inputs and GABAergic inputs into the IPN. The nature of the GABAergic inputs to the IPN is not known but could be extrinsic GABAergic inputs or local GABAergic IPN neurons themselves (56). The plasticity is associative and synapse-specific (Fig. 5 and *SI Appendix*, Fig. S6), implementing a potentially

powerful computation in the circuit. It has been suggested that IPN neurons mediate fear extinction (2). The GBR-mediated potentiation could implement a behaviorally relevant feedback loop, switching the circuit from fear responses to fear extinction.

Finally, the technological advances reported in the present paper could be useful for the analysis of transmitter release. Chemical fixation experiments (including "Flash and Fix") have several drawbacks; limited resolution for discriminating signals from the AZ and docked SV membranes, difficulty with double labeling, and long time (at least a few minutes) required for chemical fixation (57). Our Flash and Freeze-fracture method overcomes many of these limitations. First, one can easily identify proteins inserted into the AZ membrane. Second, the labeling of multiple proteins is easily achievable. Finally, it can capture molecular translocations that occur within milliseconds. Thus, the Flash and Freeze-fracture method can reveal the molecular dynamics at the AZ with the highest spatial and temporal resolution.

Overall, our study provides insights into the mechanisms underlying the unique potentiation of release by GBRs from MHb terminals and demonstrates a new regime of presynaptic modulation.

Methods

Animals. Wild-type C57BL/6J, heterozygous ChAT-ChR2-EYFP, and heterozygous ChAT-IRES-Cre mice were purchased from Jackson Laboratory. Homozygous CAPS2 KO mice were previously generated (44). SPO KO mice were generated using the CRISPR-Cas9 method. Male and female mice were used indiscriminately in all experiments. All experiments were performed in strict accordance with the license approved by the Austrian Federal Ministry of Science and Research (Animal license number: BMWFW-66.018/0012-WF/V/3b/2016) and Austrian and EU animal laws. See *SI Appendix* for a detailed description.

Electrophysiology. Acute slices were prepared as described previously (8, 58). After recovery, the slice was transferred to the recording chamber and superfused with ACSF containing 2.5 mM $CaCl_2$ and 20 μM bicuculline methiodide (Tocris, Bristol, UK) at a rate of 3 to 4 mL/min at RT (22.0 to 24.0 °C). For a detailed description, see *SI Appendix*.

Stereotaxic Surgery, AAV Injection, and Calcium Imaging. Adult ChAT-IRES-Cre mice were deeply anesthetized and placed in the stereotaxic setup. AAV9-hSynapsin1-FLEx-axon-GCaMP6s (Addgene #112010) was injected bilaterally into the MHb. For a detailed description, see *SI Appendix*.

Calcium Imaging–Based Modeling. For a detailed description, see *SI Appendix*.

Flash and Freeze and Freeze Substitution

ChAT-ChR2-EYFP mice (8 to 10 wk old) were used for Flash and Freeze and freeze substitution as described previously (18). For a detailed description, see *SI Appendix*.

Flash and Freeze-Fracture and Immunolabeling

Acutely cut IPN slices from ChAT-ChR2-EYFP mice were incubated in ACSF containing 1 mM Ca^{2+}, 1 mM TEA-Cl, and 100 μM 4-AP with or without 1 μM baclofen for 5 to 10 min. and then in the same ACSF containing 2.5 mM Ca^{2+}, 100 μM dynasore (HelloBio, Bristol, UK), and 15% PVP followed by assembly of the freezing sandwich consisting of a gold-coated copper carrier, double-sided tape, and a sapphire disc. After insertion into the ICE high-pressure freezer (Leica EM), slices were stimulated twice at 10 Hz (5-ms pulse width, 3-s duration, 10-s interval), followed by a single light pulse (8-ms duration) and high-pressure freezing, timed so that the sample reached 0 °C 8-ms after light stimulation onset. Light application continued for another 15 ms during the freezing process.

For freeze-fracture replication, the metal-sapphire sandwich was inserted into an ACE900 freeze-fracture machine (Leica EM), and the frozen tissue was fractured by moving a knife through the double-sided tape between the metal carrier and the sapphire disc. After fracture, carbon/platinum replication was performed as described previously (8). The replica-covered slices were transferred to 0.1 M phosphate buffer (PB) containing 2% PFA for postfixation for 1 h, followed by SDS treatment as described (8). For the immunolabeling procedure, see *SI Appendix*.

Immunohistochemistry and Single and Double Pre-Embedding Immunolabeling For EM

Immunohistochemistry and pre-embedding immunolabeling were performed as described previously (8). For a detailed description, see *SI Appendix*.

Flash and Fix

Coronal IPN slices (200 μm thick) of ChAT-ChR2-EYFP mice were prepared, recovered, and incubated for 10 to 15 min in ACSF containing either 2.5 mM Ca^{2+} ("Control" and "10 Hz" groups) or 2.5 mM Ca^{2+} and 1 μM baclofen ("10 Hz + Baclofen" and "Baclofen (no stimulation) groups). Each slice was then optogenetically stimulated three times at 10 Hz for 3 s (10-s interval) followed by immediate immersion fixation in 0.1 M PB containing 4% PFA, 0.05% glutaraldehyde, and 15% picric acid for 45 min. Control and "Baclofen (no stimulation)" slices were immersion-fixed without light stimulation. Thereafter, pre-embedding immunolabeling was performed as described above.

Quantification and Statistical Analysis

Unless otherwise noted, all data are presented as mean ± SEM. Parametric tests were performed unless data failed the Shapiro–Wilk normality test, in which case nonparametric tests were applied. Statistical analysis was performed in Prism 8 unless otherwise stated. For a detailed description of all data analysis procedures, see *SI Appendix*.

Data, Materials, and Software Availability. Numerical raw data of all main figures and additional representative EM images of all experiments have been deposited at ISTA REx (59).

ACKNOWLEDGMENTS. We thank Erwin Neher and Ipe Ninan for critical comments on the manuscript. This project has received funding from the European Research Council (ERC) and European Commission, under the European Union's Horizon 2020 research and innovation program (ERC grant agreement no. 694539 to R.S. and the Marie Skłodowska-Curie grant agreement no. 665385 to C.Ö.). This study was supported by the Cooperative Study Program of Center for Animal Resources and Collaborative Study of NINS. We thank Kohgaku Eguchi for statistical analysis, Yu Kasugai for additional EM imaging, Robert Beattie for the design of the slice recovery chamber for Flash and Freeze experiments, Todor Asenov from the ISTA machine shop for custom part preparations for high-pressure freezing, the ISTA preclinical facility for animal caretaking, and the ISTA EM facilities for technical support.

Author affiliations: [a]Institute of Science and Technology Austria, Klosterneuburg 3400, Austria; [b]Department of Pharmacology, Jikei University School of Medicine, Nishishinbashi, Minato-ku, Tokyo 105-8461, Japan; [c]Advanced Scientific Research Leaders Development Unit, Gunma University Graduate School of Medicine, Maebashi, Gunma 371-8511, Japan; [d]Section of Mammalian Transgenesis, National Institute for Physiological Sciences, Okazaki 444-8585, Japan; and [e]Department of Molecular Neurobiology, Max Planck Institute for Multidisciplinary Sciences, Göttingen 37077, Germany

1. H. W. Lee, S. H. Yang, J. Y. Kim, H. Kim, The role of the medial habenula cholinergic system in addiction and emotion-associated behaviors. *Front. Psychiatry* **10**, 100 (2019).
2. J. Zhang *et al.*, Presynaptic excitation via $GABA_B$ receptors in habenula cholinergic neurons regulates fear memory expression. *Cell* **166**, 716–728 (2016).
3. P. Koppensteiner, C. Galvin, I. Ninan, Development- and experience-dependent plasticity in the dorsomedial habenula. *Mol. Cell Neurosci.* **77**, 105–112 (2016).
4. M. Gassmann, B. Bettler, Regulation of neuronal $GABA_B$ receptor functions by subunit composition. *Nat. Rev. Neurosci.* **13**, 380–394 (2012).
5. J. R. Chalifoux, A. G. Carter, GABAB receptor modulation of voltage-sensitive calcium channels in spines and dendrites. *J. Neurosci.* **31**, 4221–4232 (2011).
6. T. Sakaba, E. Neher, Direct modulation of synaptic vesicle priming by GABA(B) receptor activation at a glutamatergic synapse. *Nature* **424**, 775–778 (2003).
7. B. Alten, N. J. Guzikowski, Z. Zurawski, H. E. Hamm, E. T. Kavalali, Presynaptic mechanisms underlying GABA(B)-receptor-mediated inhibition of spontaneous neurotransmitter release. *Cell Rep.* **38**, 110255 (2022).
8. P. Bhandari *et al.*, $GABA_B$ receptor auxiliary subunits modulate Cav2.3-mediated release from medial habenula terminals. *Elife* **10**, e68274 (2021).
9. R. Melani, R. Von Itter, D. Jing, P. Koppensteiner, I. Ninan, Opposing effects of an atypical glycinergic and substance P transmission on interpeduncular nucleus plasticity. *Neuropsychopharmacology* **44**, 1828–1836 (2019).
10. D. Fioravante, W. G. Regehr, Short-term forms of presynaptic plasticity. *Curr. Opin. Neurobiol.* **21**, 269–274 (2011).
11. E. Neher, N. Brose, Dynamically primed synaptic vesicle states: Key to understand synaptic short-term plasticity. *Neuron* **100**, 1283–1291 (2018).
12. H. L. Atwood, S. Karunanithi, Diversification of synaptic strength: Presynaptic elements. *Nat. Rev. Neurosci.* **3**, 497–516 (2002).
13. R. S. Zucker, W. G. Regehr, Short-term synaptic plasticity. *Annu. Rev. Physiol.* **64**, 355–405 (2002).
14. M. Aldahabi *et al.*, Different priming states of synaptic vesicles underlie distinct release probabilities at hippocampal excitatory synapses. *Neuron* **110**, 4144–4161.e7 (2022).
15. P. E. Sharp, S. Turner-Williams, S. Tuttle, Movement-related correlates of single cell activity in the interpeduncular nucleus and habenula of the rat during a pellet-chasing task. *Behav. Brain Res.* **166**, 55–70 (2006).
16. E. L. Sylwestrak *et al.*, Cell-type-specific population dynamics of diverse reward computations. *Cell* **185**, 3568–3587.e27 (2022).
17. H. Zhao, B. Rusak, Circadian firing-rate rhythms and light responses of rat habenular nucleus neurons in vivo and in vitro. *Neuroscience* **132**, 519–528 (2005).
18. C. Borges-Merjane, O. Kim, P. Jonas, Functional electron microscopy, "Flash and Freeze," of identified cortical synapses in acute brain slices. *Neuron* **105**, 992–1006.e6 (2020).
19. K. H. Lin, H. Taschenberger, E. Neher, A sequential two-step priming scheme reproduces diversity in synaptic strength and short-term plasticity. *Proc. Natl. Acad. Sci. U.S.A.* **119**, e2207987119 (2022).
20. J. Ren *et al.*, Habenula "cholinergic" neurons co-release glutamate and acetylcholine and activate postsynaptic neurons via distinct transmission modes. *Neuron* **69**, 445–452 (2011).
21. J. M. Kalkstein, K. L. Magleby, Augmentation increases vesicular release probability in the presence of masking depression at the frog neuromuscular junction. *J. Neurosci.* **24**, 11391–11403 (2004).
22. W. A. Catterall, A. P. Few, Calcium channel regulation and presynaptic plasticity. *Neuron* **59**, 882–901 (2008).
23. W. G. Regehr, Short-term presynaptic plasticity. *Cold Spring Harb. Perspect. Biol.* **4**, a005702 (2012).
24. A. Jouvenceau, F. Giovannini, C. P. Bath, E. Trotman, E. Sher, Inactivation properties of human recombinant class E calcium channels. *J. Neurophysiol.* **83**, 671–684 (2000).
25. K. Kanemaru *et al.*, Phospholipase C-eta2 is highly expressed in the habenula and retina. *Gene. Expr. Patterns* **10**, 119–126 (2010).
26. M. Nakahara *et al.*, A novel phospholipase C, PLC(eta)2, is a neuron-specific isozyme. *J. Biol. Chem.* **280**, 29128–29134 (2005).
27. G. Kabachinski, M. Yamaga, D. M. Kielar-Grevstad, S. Bruinsma, T. F. Martin, CAPS and Munc13 utilize distinct PIP2-linked mechanisms to promote vesicle exocytosis. *Mol. Biol. Cell* **25**, 508–521 (2014).
28. J. Y. Jeong, H. J. Kweon, B. C. Suh, Dual regulation of R-type CaV2.3 channels by M1 muscarinic receptors. *Mol. Cells* **39**, 322–329 (2016).
29. E. Perez-Garci, M. Gassmann, B. Bettler, M. E. Larkum, The GABAB1b isoform mediates long-lasting inhibition of dendritic Ca2+ spikes in layer 5 somatosensory pyramidal neurons. *Neuron* **50**, 603–616 (2006).
30. J. Schwenk *et al.*, Native GABA(B) receptors are heteromultimers with a family of auxiliary subunits. *Nature* **465**, 231–235 (2010).
31. L. G. Wu, P. Saggau, GABAB receptor-mediated presynaptic inhibition in guinea-pig hippocampus is caused by reduction of presynaptic Ca^{2+} influx. *J. Physiol.* **485**, 649–657 (1995).
32. Y. Zhang, L. L. Looger, Fast and sensitive GCaMP calcium indicators for neuronal imaging. *J. Physiol.*, 10.1113/JP283832 (2023).
33. E. Eggermann, I. Bucurenciu, S. P. Goswami, P. Jonas, Nanodomain coupling between Ca^{2+} channels and sensors of exocytosis at fast mammalian synapses *Nat. Rev. Neurosci.* **13**, 7–21 (2011).
34. E. Neher, Merits and limitations of vesicle pool models in view of heterogeneous populations of synaptic vesicles. *Neuron* **87**, 1131–1142 (2015).
35. R. Schneggenburger, A. C. Meyer, E. Neher, Released fraction and total size of a pool of immediately available transmitter quanta at a calyx synapse. *Neuron* **23**, 399–409 (1999).
36. P. S. Kaeser, W. G. Regehr, The readily releasable pool of synaptic vesicles. *Curr. Opin. Neurobiol.* **43**, 63–70 (2017).
37. C. Imig *et al.*, The morphological and molecular nature of synaptic vesicle priming at presynaptic active zones. *Neuron* **84**, 416–431 (2014).
38. G. Nagel *et al.*, Channelrhodopsin-2, a directly light-gated cation-selective membrane channel. *Proc. Natl. Acad. Sci. U.S.A.* **100**, 13940–13945 (2003).
39. A. Berndt *et al.*, High-efficiency channelrhodopsins for fast neuronal stimulation at low light levels. *Proc. Natl. Acad. Sci. U.S.A.* **108**, 7595–7600 (2011).
40. B. Kolisnyk *et al.*, ChAT-ChR2-EYFP mice have enhanced motor endurance but show deficits in attention and several additional cognitive domains. *J. Neurosci.* **33**, 10427–10438 (2013).
41. I. Singec *et al.*, Synaptic vesicle protein synaptoporin is differently expressed by subpopulations of mouse hippocampal neurons. *J. Comp. Neurol.* **452**, 139–153 (2002).
42. P. Knaus, B. Marqueze-Pouey, H. Scherer, H. Betz, Synaptoporin, a novel putative channel protein of synaptic vesicles. *Neuron* **5**, 453–462 (1990).
43. C. S. Müller *et al.*, Quantitative proteomics of the Cav2 channel nano-environments in the mammalian brain. *Proc. Natl. Acad. Sci. U.S.A.* **107**, 14950–14957 (2010).
44. W. J. Jockusch *et al.*, CAPS-1 and CAPS-2 are essential synaptic vesicle priming proteins. *Cell* **131**, 796–808 (2007).
45. T. Sadakata *et al.*, Impaired cerebellar development and function in mice lacking CAPS2, a protein involved in neurotrophin release. *J. Neurosci.* **27**, 2472–2482 (2007).
46. Y. Shinoda *et al.*, Calcium-dependent activator protein for secretion 2 (CAPS2) promotes BDNF secretion and is critical for the development of GABAergic interneuron network. *Proc. Natl. Acad. Sci. U.S.A.* **108**, 373–378 (2011).
47. T. Sadakata *et al.*, Differential distributions of the Ca^{2+}-dependent activator protein for secretion family proteins (CAPS2 and CAPS1) in the mouse brain. *J. Comp. Neurol.* **495**, 735–753 (2006).
48. S. Tabata *et al.*, Electron microscopic detection of single membrane proteins by a specific chemical labeling. *iScience* **22**, 256–268 (2019).
49. J. M. Bekkers, J. D. Clements, Quantal amplitude and quantal variance of strontium-induced asynchronous EPSCs in rat dentate granule neurons. *J. Physiol.* **516**, 227–248 (1999).
50. A. G. Millar, R. S. Zucker, G. C. Ellis-Davies, M. P. Charlton, H. L. Atwood, Calcium sensitivity of neurotransmitter release differs at phasic and tonic synapses. *J. Neurosci.* **25**, 3113–3125 (2005).
51. D. C. Crawford, E. T. Kavalali, Molecular underpinnings of synaptic vesicle pool heterogeneity. *Traffic* **16**, 338–364 (2015).
52. D. M. Ramirez, E. T. Kavalali, Differential regulation of spontaneous and evoked neurotransmitter release at central synapses. *Curr. Opin. Neurobiol.* **21**, 275–282 (2011).
53. M. Bera *et al.*, Synaptophysin chaperones the assembly of 12 SNAREpins under each ready-release vesicle. *Proc. Natl. Acad. Sci. U.S.A.* **120**, e2311484120 (2023).
54. D. R. Stevens, J. Rettig, The Ca^{2+}-dependent activator protein for secretion CAPS: Do I dock or do I prime? *Mol. Neurobiol.* **39**, 62–72 (2009).
55. C. Q. Nguyen Truong *et al.*, Secretory vesicle priming by CAPS is independent of its SNARE-binding MUN domain. *Cell Rep.* **9**, 902–909 (2014).
56. S. Molas, S. R. DeGroot, R. Zhao-Shea, A. R. Tapper, Anxiety and nicotine dependence: Emerging role of the habenulo-interpeduncular axis. *Trends Pharmacol. Sci.* **38**, 169–180 (2017).
57. N. Korogod, C. C. Petersen, G. W. Knott, Ultrastructural analysis of adult mouse neocortex comparing aldehyde perfusion with cryo fixation. *Elife* **4**, e05793 (2015).
58. T. Vega-Zuniga, D. Trost, K. Schicker, E. M. Bogner, H. Luksch, The medial ventrothalamic circuitry: Cells implicated in a bimodal network. *Front. Neural. Circuits* **12**, 9 (2018).
59. R. Shigemoto, Transition from tonic to phasic neurotransmitter release by presynaptic GABAB receptor activation in medial habenula terminals. ISTA REx. https://doi.org/10.15479/AT:ISTA:13173. Deposited 29 July 2023.